



# Examination of the electroactive composites containing cobalt nanoclusters and nitrogen-doped nanostructured carbon as electrocatalysts for oxygen reduction reaction

Aleksandra Pacuła<sup>a,b,c,\*</sup>, Katsuyoshi Ikeda<sup>b,d</sup>, Takuya Masuda<sup>b,d</sup>, Kohei Uosaki<sup>a,b,d</sup>

<sup>a</sup> International Center for Materials Nanoarchitectonics (WPI-MANA), National Institute for Materials Science (NIMS), 1-1 Namiki, Tsukuba, Ibaraki 305-0044, Japan

<sup>b</sup> Division of Chemistry, Graduate School of Science, Hokkaido University, Sapporo 060-0810, Japan

<sup>c</sup> Jerzy Haber Institute of Catalysis and Surface Chemistry, Polish Academy of Sciences, Niezapominajek 8, 30-239 Kraków, Poland

<sup>d</sup> Global Research Center for Environment and Energy based on Nanomaterials Science (GREEN), National Institute for Materials Science (NIMS), 1-1 Namiki, Tsukuba, Ibaraki 305-0044, Japan

## HIGHLIGHTS

- The electroactive composites are prepared by a simple and inexpensive method.
- Synthesis temperature affects metallic Co size, level of N-doping and graphitization.
- The electrocatalysts are active in oxygen reduction reaction in alkaline solution.

## ARTICLE INFO

### Article history:

Received 3 May 2012

Received in revised form

13 July 2012

Accepted 26 July 2012

Available online 4 August 2012

### Keywords:

Carbon nanotube

Layered double hydroxides

Electrocatalyst

Composite

Catalytic chemical vapour deposition

Oxygen reduction reaction

## ABSTRACT

A series of electroactive composites containing cobalt nanoclusters and N-doped graphite-like carbon is obtained by catalytic chemical vapour deposition (CCVD) using Mg–Co–Al layered double hydroxides and acetonitrile. The influence of synthesis temperature, e.g. 600, 700 and 800 °C on their physico-chemical properties is examined by means of X-ray diffraction, elemental analysis, thermal analysis, nitrogen sorption, Raman spectroscopy, X-ray photoelectron spectroscopy, scanning and transmission electron microscopy.

N-doped graphite-like carbon in the catalysts shows various morphologies. The composite prepared at 600 °C contains plate-like particles, whereas those synthesized at 700 and 800 °C, contain not only plate-like particles but also multi-walled carbon nanotubes. The concentration of nitrogen uniformly incorporated in the carbon framework is ca. 2 wt %.

The electrocatalytic properties of the catalysts for oxygen reduction reaction (ORR) are evaluated in alkaline media by cyclic voltammetry and rotating disk electrode (RDE) measurement. The composites are proved to have the ability to reduce oxygen according to 2-electron pathway.

© 2012 Elsevier B.V. All rights reserved.

## 1. Introduction

Electrochemical devices such as fuel cells, secondary batteries and capacitors are the key to establish a sustainable society and the aim of the present study was to create electroactive composites, which may serve as electrode materials for electrochemical devices, therefore, they should be electrically conductive, porous and electrocatalytically active. To accomplish these objectives we selected two key components, namely cobalt nanoclusters and nitrogen

(N)-doped nanostructured carbon. The choice of these constituents was guided by previous works that have shown the beneficial effects of using similar composition on the activity of the electrode materials [1–8]. There is currently an intense interest in the development of non-precious metal electrocatalysts. Although transition metal catalysts, particularly containing Co and Fe, attract much interest as electrocatalysts for oxygen reduction reaction (ORR) [2,3,9–14], N-doped carbon nanostructures have been also reported to show enhanced catalytic activity towards ORR [15–23].

Here we report the synthesis and characterization of the electrocatalysts containing cobalt species and N-doped nanostructured carbon, which were obtained via catalytic chemical vapour deposition (CCVD) at 600, 700 and 800 °C using Mg–Co–Al layered double hydroxides (LDHs) and acetonitrile as starting materials. We

\* Corresponding author. Jerzy Haber Institute of Catalysis and Surface Chemistry, Polish Academy of Sciences, Niezapominajek 8, 30-239 Kraków, Poland. Tel.: +48 12 6395131; fax: +48 12 4251923.

E-mail address: [ncpacula@cyfronet.pl](mailto:ncpacula@cyfronet.pl) (A. Pacuła).

demonstrate that thermal decomposition of organic compound containing nitrogen (acetonitrile) in the presence of transition metal (cobalt) is a simple method of carbonization and N-doping, whereas LDHs are inexpensive metal precursors for the preparation of carbon nanostructures [4,24–27]. Contrary to the previous works, we used as-prepared LDHs, which were obtained under mild hydrothermal conditions, e.g. at room temperature, in air, and with short ageing, without calcination and reduction before CCVD. Selection of cobalt as one of the components in the electroactive composites has a big advantage because it can perform two catalytic functions, in the formation of carbon nanostructure during the synthesis of the composites, and towards oxygen reduction during the application of the electrocatalysts [4,9,27].

The present work provides a convenient single-step synthesis method of the electrode materials with ORR activity comparable to those containing Co species deposited on graphene [2] or Pt particles spread on carbon nanotubes [17] and is an important contribution to the formation of carbon nanotubes by application of Co-based LDHs.

## 2. Experimental

### 2.1. Materials

Magnesium nitrate hexahydrate ( $\text{Mg}(\text{NO}_3)_2 \cdot 6\text{H}_2\text{O}$ , JIS special grade), cobalt (II) nitrate hexahydrate ( $\text{Co}(\text{NO}_3)_2 \cdot 6\text{H}_2\text{O}$ , JIS special grade), aluminium nitrate nonahydrate ( $\text{Al}(\text{NO}_3)_3 \cdot 9\text{H}_2\text{O}$ , 99.9%), sodium hydroxide (NaOH, JIS special grade), potassium hydroxide (KOH, JIS special grade), acetone ( $(\text{CH}_3)_2\text{CO}$ , 99.0%) were purchased from Wako Pure Chemical Industries, Ltd. All chemicals were used as received. Alumina polishing suspension (particle size, 0.35  $\mu\text{m}$ ) was purchased from Baikowski International Corporation. Nafion® PFSA Polymer Dispersion DE 2020 was purchased from DuPont Fuel Cells. Nitrogen ( $\text{N}_2$ , 99.99%) was purchased from Air Water, whereas other gases, e.g. argon (Ar, 99.999%) and oxygen ( $\text{O}_2$ , 99.8%) were purchased from Suzuki Shokan. Water was purified using a Milli-Q purification system (Millipore).

### 2.2. Preparation of the composites

Mg–Co–Al LDHs (with Mg:Co:Al atomic ratio of 1.75:0.25:1) were synthesized by a co-precipitation method. Aqueous solutions of sodium hydroxide and a mixture of magnesium, cobalt and aluminium nitrates were simultaneously added dropwise to deionized water at constant pH of 10. Hydrothermal synthesis and ageing were carried out at room temperature for 30 min. Then the slurry was filtered, washed with deionized water and dried overnight at 50 °C.

The composites were prepared as follows: 1 g of Mg–Co–Al LDHs in an alumina boat was placed in a tube furnace and heated under a flow of nitrogen ( $30 \text{ mL min}^{-1}$ ) to the required temperature (600, 700 and 800 °C). Then the nitrogen stream was saturated with acetonitrile vapour and the sample maintained at the target temperature for 3 h. The composites were cooled down under a flow of nitrogen.

### 2.3. Characterization of the composites

Powder X-ray diffraction (XRD) analysis was performed using a MultiFlex Rigaku powder diffractometer with Cu  $K_\alpha$  radiation (40 kV, 20 mA). The XRD patterns were recorded in the range of 5–139° at scan rate of  $4.8^\circ \text{ min}^{-1}$  with a step size of  $0.05^\circ$ . Elemental analysis was carried out using a CHNS analyzer (MICRO CORDER JM10). Thermogravimetric (TG) analysis was performed using a Thermo plus TG8120 (Rigaku) analyzer up to 1000 °C

under static air condition with a heating rate of  $5^\circ \text{C min}^{-1}$ . Raman spectroscopic measurements were conducted by 0.7 mW 632.8 nm excitation. Nitrogen adsorption/desorption analysis was carried out at  $-196^\circ \text{C}$  using an Autosorb-6B, Quantachrome surface area and pore size analyzer. Prior to volumetric sorption measurement, the samples were preheated and degassed under vacuum at 100 °C for 4 h. Scanning electron microscopy (SEM) and transmission electron microscopy (TEM) images were recorded using an HD-2000 microscope (Hitachi) with an operating voltage of 200 keV. X-ray photoelectron spectroscopic (XPS) measurements were performed using an XPS-7000 spectrometer (Rigaku) equipped with Mg  $K_\alpha$  X-ray source.

### 2.4. Electrochemical measurement

Glassy carbon (GC) was used as a substrate for electrochemical measurements. A GC substrate was polished by aqueous alumina suspension on a polishing cloth, and then cleaned by ultrasonic treatment in Milli-Q water and acetone. The composites (20 mg) were ultrasonically mixed with 1 wt % Nafion suspension (1.5 mL) for 60 min. Then the resulting suspension (5  $\mu\text{L}$ ) was spread on a GC disk (5 mm in diameter) and dried in air at room temperature. The composite loading was  $0.35 \text{ mg cm}^{-2}$ .

Electrochemical measurements were performed with an automatic polarization system (Hokuto Denko, HSV-100) using a conventional three-electrode configuration electrochemical cell. A Pt wire and a Ag/AgCl/NaCl<sub>sat</sub> were used as a counter and reference electrode, respectively. Cyclic voltammograms were recorded at sweep rates of 5, 10, 20, 50, 100  $\text{mV s}^{-1}$ . Rotating disk electrode (RDE) measurements were carried out using a dynamic electrode unit (Hokuto Denko, HR-201 and HR-202). Current-potential relations were recorded at a sweep rate of  $5 \text{ mV s}^{-1}$  with rotation rate from 400 to 1600 rpm. The electrolyte was 0.1 M KOH aqueous solution saturated with either oxygen or argon. The bubbling time with oxygen or argon was roughly 40 min. All the electrochemical experiments were carried out at  $25 \pm 1^\circ \text{C}$ . All given potentials are referred to Ag/AgCl/NaCl (sat'd).

## 3. Results and discussion

### 3.1. Powder X-ray diffraction and elemental analysis

Fig. 1 shows the XRD patterns of the composites prepared at 600, 700 and 800 °C. XRD analysis reveals that all the composites are composed of several components, which are the products of thermal decomposition of Mg–Co–Al LDHs and acetonitrile. According to XRD results, the composite prepared at 600 °C contains two crystalline phases of cobalt oxide with characteristic XRD reflections at  $2\theta = 35.3, 43.5, 61.1^\circ$  [28] and magnesium oxide

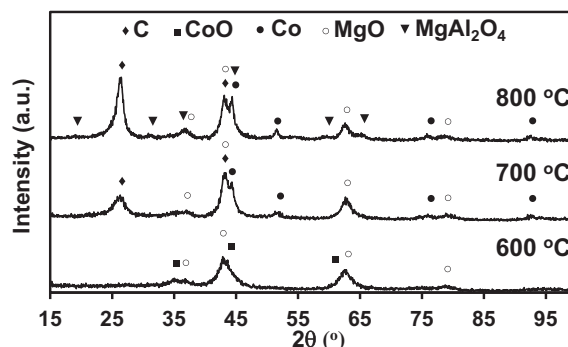


Fig. 1. The XRD patterns of the composites prepared at 600, 700 and 800 °C.

with characteristic XRD reflections at  $2\theta = 37.2, 43.2, 62.7, 79.8^\circ$  [29]. Whereas the composite prepared at  $700^\circ\text{C}$  contains three crystalline phases of metallic cobalt with characteristic XRD reflections at  $2\theta=44.3, 51.9, 76.0, 93.1^\circ$  [30], magnesium oxide and turbostratic/graphitic carbon with typical XRD reflections at  $2\theta=25.9, 43.3^\circ$  [31]. The composite synthesized at  $800^\circ\text{C}$  contains four crystalline phases of metallic cobalt, magnesium oxide, turbostratic/graphitic carbon and magnesium aluminium oxide with characteristic XRD peaks at  $2\theta=19.3, 31.6, 37.3, 44.4, 60.0, 65.4^\circ$  [32]. Overall, synthesis temperature has a great influence on the phase composition, the relative contribution of the components and the level of crystallinity.

It is likely that before the introduction of acetonitrile into synthesis reaction, cobalt species derived from Mg–Co–Al LDHs occur only in the form of oxides. Then, during CCVD, cobalt oxides are subsequently reduced through the decomposition of  $\text{CH}_3\text{CN}$  to metallic cobalt [20,22]. It seems that the concentration of metallic cobalt in the composites increases with increasing CCVD temperature, which affects the intensity of the reflections in the XRD pattern. Moreover, metallic cobalt particles undergo clustering at elevated temperature leading to an increase in Co particles size, which influences the width of the reflections in the XRD pattern. As a consequence of increasing CCVD temperature, the diffraction peaks assigned to metallic cobalt become higher and narrower reflecting differences in the amount of metallic cobalt phase and changes in metal particle size.

CNH compositions of the composites prepared at various temperatures determined by elemental analysis are summarized in Table 1. While the carbon content in the composites increases significantly, the nitrogen content slightly decreases as synthesis temperature increases. These results are in agreement with the fact that heteroatoms are eliminated from the carbon framework at higher temperature [33].

### 3.2. Thermogravimetric analysis

Fig. 2 shows (a) thermogravimetric (TG) and (b) differential thermogravimetric (DTG) profiles of the composites prepared at  $600, 700$  and  $800^\circ\text{C}$ . All the composites exhibit a single mass loss event occurring between  $270$  and  $450^\circ\text{C}$ , which may be ascribed to the combustion of the carbon component. Therefore, the magnitude of the mass loss may be considered as being approximately equal to the carbon content in the composites. The carbon content in the composites, e.g.  $14, 38$  and  $57\text{ wt } \%$ , increases with increasing synthesis temperature, e.g.  $600, 700$  and  $800^\circ\text{C}$ , respectively. These results are in agreement with the data obtained from elemental analysis (Table 1). In addition, thermal analysis indicates that the onset temperature for the combustion of the carbon component gradually increases as synthesis temperature becomes higher. Moreover, DTG profiles (Fig. 2b) illustrate that the temperature of the mass loss maximum shifts towards higher values from  $340$  via  $380$ – $400^\circ\text{C}$  for the composites prepared at  $600, 700$  and  $800^\circ\text{C}$ , respectively. An increase in the combustion temperature implies a higher degree of graphitization of the carbon component in the composites

prepared at higher temperatures [34], which is also confirmed by XRD analysis. These results are consistent with observations of Jiang et al. [35], which indicate that thermal decomposition temperature for graphite increases as its average particle size increases and the fraction of edge plane sites decreases. Therefore an observed increase in the combustion temperature of the carbon component implies a decrease in the density of edge plane sites in the carbon framework.

### 3.3. Raman spectroscopy

Differences in the structural ordering of the carbon component in the composites are assessed by means of Raman spectroscopy. Fig. 3 displays the Raman spectra of the composites. All the spectra show two broad bands centered at about  $1340$  and  $1590\text{ cm}^{-1}$ , which can be assigned to the D-band and G-band, which are characteristic of disordered and ordered graphitic lattice, respectively [20].

In general, the D-band corresponds to defects, impurities or lattice distortions in graphitic ordering, while the G-band indicates the degree of crystallinity in graphitic structure. The presence of both bands in the Raman spectra confirms that the carbon-rich constituent is a combination of both structural orderings, which is typically observed for turbostratic carbon.

According to the literature, in N-doped carbon materials nitrogen creates defects in carbon layers leading to a certain increase in edge plane exposure [22]. Disruptions and irregular curvature in graphene stacking in N-doped carbons are related to the propensity of incorporated nitrogen that forms pentagonal defects in the graphene sheets. The introduction of pentagons into the basal planes disrupts the planar hexagonal arrangement of carbon atoms found in graphite, causes buckling of the graphene layers, and results in interlayer distances that fluctuate between wider and thinner distances than found in pristine graphite [23]. Therefore N-doping may be responsible for the roughness of walls [26].

It is noticed for the composites prepared at higher temperatures that the intensity of the G-band increases, whereas the intensity of the D-band decreases as a consequence of a higher extent of graphitization and a lower number of defects in the carbon framework resulted also from decreasing nitrogen content. This conclusion is in agreement with XRD. Moreover, the G-band for the composites prepared at  $600$  and  $700^\circ\text{C}$  is slightly shifted to higher wavenumbers (reflecting in asymmetric shape) in comparison to that for the composite prepared at  $800^\circ\text{C}$ . This shift can be explained by the contraction of the lattice spacing is related to the formation of C–N bonds, which increases the size of the Brillouin zone. Therefore, the stretching of in-plane covalent bonds is stronger, resulting in the shift of the G-band to higher frequency [20].

### 3.4. Nitrogen sorption

Nitrogen sorption measurements reveal that the composites have different porosity. The nitrogen sorption isotherms of the composites shown in Fig. 4, can be classified as type IV with type H2 hysteresis loop for the composite prepared at  $600^\circ\text{C}$  or as type III with no hysteresis loop for the composites prepared at  $700$  and  $800^\circ\text{C}$  [36]. It implies that the composite prepared at  $600^\circ\text{C}$  is mesoporous, whereas the composites prepared at  $700$  and  $800^\circ\text{C}$  are macroporous.

Differences in porosity of the composites are also reflected in the average pore size that is  $5, 31$  and  $27\text{ nm}$  for the composites prepared at  $600, 700$  and  $800^\circ\text{C}$ , respectively (Table 2). It reveals that the composites prepared at  $700$  and  $800^\circ\text{C}$  in addition to

**Table 1**

Bulk (calculated from elemental analysis) CNH composition of the composites prepared at various temperatures.

CCVD temp.	Bulk concentration (wt %)			
	C	N	H	C + N + H
$600^\circ\text{C}$	10.6	2.3	1.1	14.0
$700^\circ\text{C}$	35.0	1.7	0.7	37.4
$800^\circ\text{C}$	52.0	1.5	0.5	54.0

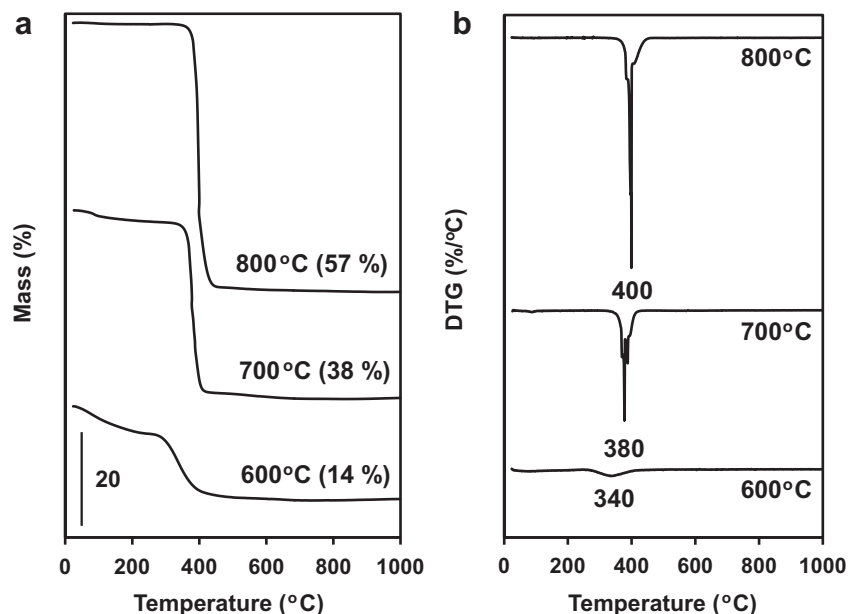


**Fig. 2.** (a) Thermogravimetric (TG) curves and (b) corresponding differential thermogravimetric (DTG) profiles of the composites prepared at 600, 700 and 800 °C. Values in parentheses in (a) are the magnitudes of mass loss at between 270 and 450 °C.

macropores with diameter above 50 nm contain also mesopores with diameter in the range of 2–50 nm.

Changes in structural ordering of the constituents cause a sharp drop in specific surface area and pore volume of the composites. Specific surface area decreases from 116 m<sup>2</sup> g<sup>-1</sup> for the composite

prepared at 600 °C to 9 and 13 m<sup>2</sup> g<sup>-1</sup> for the composites prepared at 700 and 800 °C, respectively. Pore volume changes from 0.14 cm<sup>3</sup> g<sup>-1</sup> for the composite prepared at 600 °C to 0.07 and 0.08 cm<sup>3</sup> g<sup>-1</sup> for the composites prepared at 700 and 800 °C, respectively.

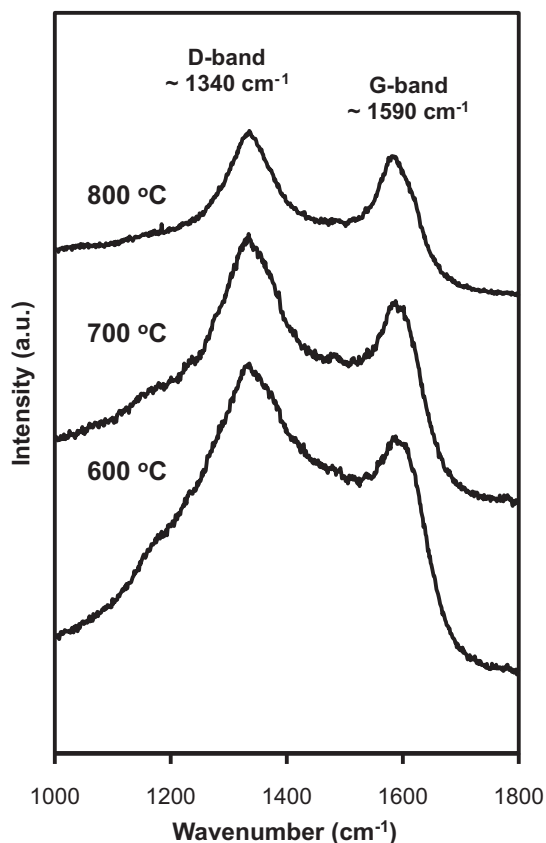


**Fig. 3.** Raman spectra of the composites prepared at 600, 700 and 800 °C.

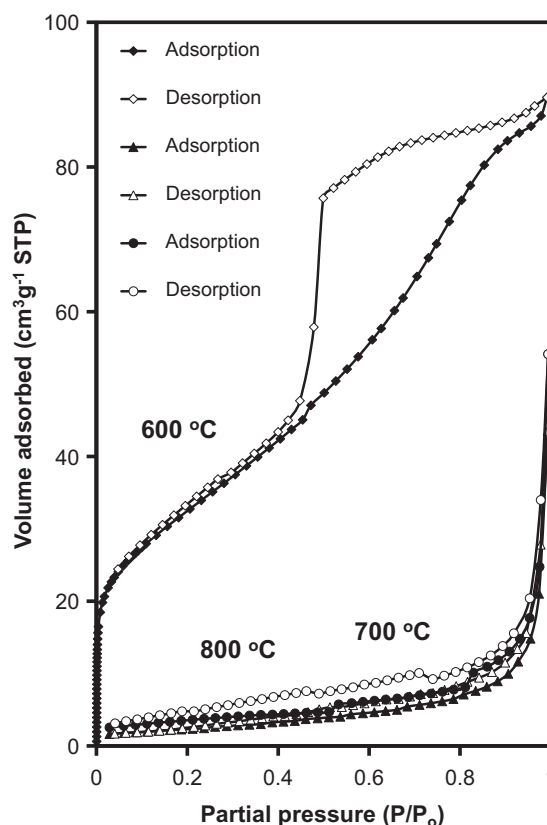


**Fig. 4.** Nitrogen sorption isotherms of the composites prepared at 600, 700 and 800 °C.

**Table 2**  
The textural properties of the composites.

CCVD temp.	Specific surface area (m <sup>2</sup> g <sup>-1</sup> )	Pore volume (cm <sup>3</sup> g <sup>-1</sup> )	Pore size (nm)
600 °C	116 ± 2%	0.14	5
700 °C	9 ± 4%	0.07	31
800 °C	13 ± 2%	0.08	27

### 3.5. Scanning and transmission electron microscopy

Changes in the textural properties of the composites prepared at various temperatures may not only be related to an increase in the level of crystallinity but also to differences in their morphology. SEM and TEM images of the composites, shown in Figs. 5 and 6, respectively, indicate that the composites consist of large aggregates of either oriented platelets for the sample prepared at 600 °C or plate-like particles and a mixture of straight, curly, coiled carbon nanotubes for the composites synthesized at 700 and 800 °C. The possible explanation for the lack of carbon nanotubes in the sample prepared at 600 °C may be the absence of sufficient amount of accessible metallic cobalt for carbon nanotubes growing. Analysis of the XPS spectrum of the sample prepared at 600 °C confirms that majority of cobalt species occurs as cobalt oxide, which indeed is inactive towards the formation of carbon nanotubes. Both composites prepared at higher temperatures contain defective multi-walled CNTs with spaghetti-like appearance, which is characteristic of CNTs grown via catalytic chemical vapour deposition route [37].

CNTs synthesized at lower temperature (700 °C) have smaller diameters, in the range of 30–120 nm, whereas those synthesized at higher temperature (800 °C) have larger diameters, in the range of 50–400 nm. The average diameter of CNTs increases with raising synthesis temperature. In general, the diameter of carbon nanotubes is determined by the size of catalyst particles, e.g. Co nanoclusters [38].

According to XRD analysis (Fig. 1), the composites prepared at various temperatures contain metallic cobalt particles different in size. Larger metal particles are a consequence of clustering of smaller metal particles at elevated temperature.

### 3.6. X-ray photoelectron spectroscopy

XPS analysis indicates the presence of carbon, nitrogen, magnesium, aluminum, cobalt, oxygen in the external part of the composites (Table 3). The most prevalent element at the surface of the composites is carbon. The surface carbon concentration is 40.2, 71.3 and 79.0 wt % for the composites prepared at 600, 700 and 800 °C, respectively. The carbon concentration increases with increasing synthesis temperature which is consistent with elemental analysis data (Table 1). C 1s signal in the XPS spectra shown in Fig. 7 may consist of five components such as C=C (285 eV), C–N, C–O, (286 eV) C=N, C=O (287 eV), COO (289 eV),

OCO (290 eV) [39]. C=C component characteristic of graphite makes a main contribution to C 1s signal.

XPS data vividly reflect changes in surface elemental composition of the composites. A gradual decrease in the intensity of Mg 2p, Al 2p and O 1s signals illustrates a subsequent covering of metal oxides derived from Mg–Co–Al LDHs by the carbon deposit. According to the XPS spectra shown in Fig. 7, Mg 2p asymmetric signal may consist of two components, namely magnesium oxide (51 eV) and magnesium aluminium oxide (55 eV) [40,41]. Analysis of XPS spectra displayed in Fig. 7 reveals that Al 2p asymmetric signal may consist of three components such as low-energy aluminium oxide (73 eV) covered with the carbon coating and high-energy aluminium oxide (75 eV) the carbon coating free [42]. It is worth to mention that aluminium oxide in the composites exists in amorphous phase and therefore cannot be detected by XRD analysis. Third component of Al 2p signal may be attributed to magnesium aluminium oxide (78 eV), which is evidenced by XRD analysis only for the composite prepared at 800 °C. The surface aluminium concentration drops drastically from 19.7 wt % for the composite prepared at 600 °C to 4.1 and 0.7 wt % for the composites prepared at 700 and 800 °C, respectively. It shows that during the formation of the composites, metal oxide grains are almost completely covered with increasing amount of the carbon component.

According to the XPS spectra shown in Fig. 7, O 1s asymmetric signal for the composite prepared at 600 °C may consist of four components such as cobalt oxide (530 eV), magnesium oxide (531 eV), aluminium oxide (532 eV) and magnesium aluminium oxide (534 eV) [40,41,43]. For the composites prepared at higher temperatures of 700 and 800 °C, O 1s signal becomes less intense and additionally its position is shifted. The surface oxygen concentration decreases from 26.3 wt % for the composite prepared at 600 °C to 15.5 and 10.0 wt % for the composites prepared at 700 and 800 °C, respectively. O 1s signal for the composites prepared at higher temperature may consist of five components characteristic of oxygen containing groups being incorporated into the carbon framework such as C=O (531 eV), C–OH (533 eV), C–O–C (534 eV), –COO (535 eV) and adsorbed water molecules (536 eV) [39,44].

Analysis of the XPS spectra shown in Fig. 7, reveals that Co 2p signal for the composite prepared at 600 °C may consist of two components, namely metallic cobalt (2p<sub>3/2</sub> = 778 eV; 2p<sub>1/2</sub> = 793 eV) and cobalt oxide (2p<sub>3/2</sub> = 782 eV; 2p<sub>1/2</sub> = 798 eV) [45–47]. Co 2p signal for metallic cobalt does not exhibit shake-up satellites lines, whereas for the compounds containing Co<sup>2+</sup> exhibits intense shake-up satellites lines located at about 4–5 eV above the main XPS line [48]. Co 2p signal for the composites prepared at 700 and 800 °C consists only of metallic cobalt component. XPS data indicate that cobalt oxide is a dominant phase containing cobalt in the sample synthesized at 600 °C, whereas in the samples obtained at higher temperatures (700 and 800 °C) metallic cobalt is an only phase containing cobalt, which is also evidenced by XRD analysis. The surface cobalt concentration is 1.6, 0.1 and 0.2 wt % for the composites prepared at 600, 700 and 800 °C, respectively, and decreases for the composites prepared at

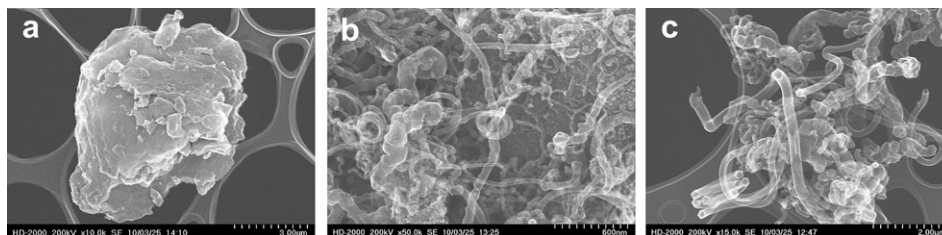


**Fig. 5.** SEM images of the composites prepared at (a) 600, (b) 700 and (c) 800 °C.

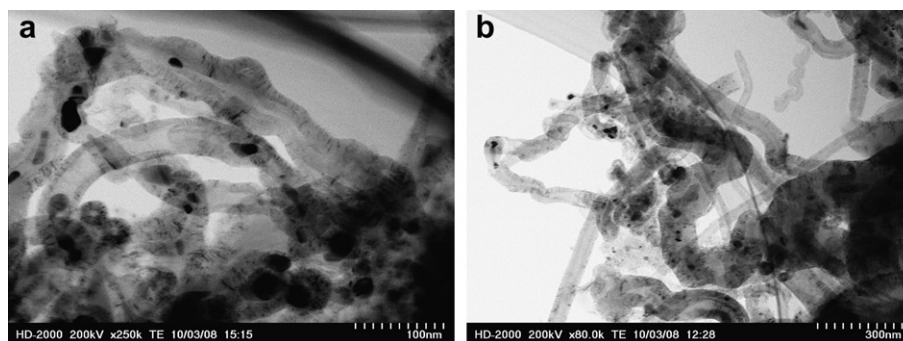


Fig. 6. TEM images of the composites prepared at (a) 700 and (b) 800 °C.

higher temperatures as a result of being covered with an increasing amount of the carbon deposit and also as a consequence of being deeply embedded in carbon nanostructures. SEM and TEM images clearly illustrate that in the composites prepared at 700 and 800 °C, cobalt particles are encapsulated in carbon nanotubes.

According to the XPS spectra shown in Fig. 7, the surface nitrogen concentration is 2.1, 1.7 and 1.6 wt % for the composites prepared at 600, 700 and 800 °C, respectively. N 1s signal may consist of four components ascribed to pyridinic nitrogen (399 eV), pyrrolic nitrogen (401 eV), quaternary nitrogen (401 eV) and oxidized nitrogen (404 eV) [19].

The surface nitrogen content is very close to the bulk nitrogen content (1.5–2.3 wt %) calculated from elemental analysis (Table 1). This implies that nitrogen is uniformly distributed throughout the N-doped carbon framework.

### 3.7. Electrochemical characteristics

Among newly prepared composites, those synthesized at 700 and 800 °C are chosen for electrochemical examination because we are not able to prepare a GC electrode coated with the composite prepared at 600 °C.

Fig. 8 shows the CV recorded in 0.1 M KOH solution saturated either with argon or oxygen at a bare GC (a) and GC coated with the electrocatalysts prepared at 700 (b) and 800 °C (c). The CVs recorded in an argon-saturated solution are featureless and almost rectangular in shape, showing the currents associated with charging of the electrical double layer. The charging currents at a GC electrode coated with the composites are higher than that at a bare GC. The capacitances for the composites prepared at 700 and 800 °C are ca. 7 and 4 F g<sup>−1</sup>, respectively. The composite synthesized at lower temperature exhibits higher capacitance as it is less compact and indicates a lower degree of crystallinity, resulting in larger interface area. Its enhanced capacitive performance may also result from higher contribution of the edge plane surface than the basal plane surface [49].

In the CVs recorded in 0.1 M KOH solution saturated with oxygen, a single reduction peak corresponding to the reduction of oxygen is observed. The CVs of 1st, 2nd and 3rd sweep are shown to illustrate that the peak current decreases gradually during ORR as

a result of oxygen deficiency in the catalyst pores. In addition, the peak current varies linearly with the square root of the potential scan rate (the data not shown) suggesting that the electrocatalytic reduction of oxygen at catalyst-coated GC electrodes is a diffusion-controlled process. Only cathodic peak is observed and no anodic peak is noticed in all the CVs recorded in oxygen-saturated 0.1 M KOH solution, which implies that the reduction of oxygen at these electrodes is an irreversible process. The oxygen reduction peaks are observed at −0.19 and −0.22 V in the CVs recorded for the samples prepared at 700 and 800 °C, respectively. These results are comparable with previous results reported for N-doped carbon nanostructures, e.g. nanotubes, nanofibers and also for other electrocatalytic systems, e.g. containing Pt deposited on carbon nanotubes or Co species spread on graphene [1,2,17,18,23]. The reduction peak shifts to more negative potential for the catalyst prepared at higher temperature. Similar trend in the shift of the peak potential towards more negative for the electrocatalysts prepared at higher temperature is reported by Qin et al. [10].

In order to obtain more insight into the behavior of the catalysts towards ORR, a rotating disk electrode technique is applied and the current–potential relations are recorded at a scan rate of 5 mV s<sup>−1</sup> with rotation rate changing from 400 to 1600 rpm.

Fig. 9 shows the current–potential relations obtained in oxygen-saturated 0.1 M KOH solution for a GC coated with the composites prepared at 700 (a) and 800 °C (b). In both cases, cathodic current starts to flow at around −0.15 V, increases as potential becomes negative. Current is not dependent on the rotation rate at less negative potentials, showing that the ORR rate is kinetically controlled, but becomes rotation rate dependent, reflecting the contribution of the transport of oxygen, as potential becomes more negative. Current reaches rotation rate dependent limiting value when potential becomes sufficiently negative.

The RDE data in the limiting current regime are analyzed using the Levich equation to determine the number of electrons per oxygen molecule, *n*, transferred in the overall reaction process [50]:

$$i = 0.62nFAD^{2/3}C_v^{-1/6}\omega^{1/2} = B\omega^{1/2}$$

where *i* is the measured limiting current, *F* is the Faraday's constant (96,485 C mol<sup>−1</sup>), *A* is the geometric electrode area (0.20 cm<sup>2</sup>), *D* and *C* are the diffusion coefficient of dissolved oxygen (1.9 × 10<sup>−5</sup> cm<sup>2</sup> s<sup>−1</sup>) and the concentration of dissolved oxygen (1.2 × 10<sup>−6</sup> mol cm<sup>−3</sup>) in 0.1 M KOH, respectively; *v* is the kinematic viscosity of the electrolyte solution (0.01 cm<sup>2</sup> s<sup>−1</sup>), and *ω* is the rotation rate (rad s<sup>−1</sup>) [51].

Levich plots (*i* versus *ω*<sup>1/2</sup>) for the measured limiting current at −0.6 and −0.7 V for the catalysts prepared at 700 and 800 °C, respectively, are shown in Fig. 10. Experimentally obtained currents are on the theoretical linear line with *ω*<sup>1/2</sup> for *n* = 2 when rotation rate is low but deviate from the linear relation with *ω*<sup>1/2</sup> as rotation rate

Table 3

Surface (derived from XPS analysis) chemical composition of the composites prepared at various temperatures.

CCVD temp.	Surface concentration (wt %)					
	C	N	Mg	Al	Co	O
600 °C	40.2	2.1	10.2	19.7	1.6	26.3
700 °C	71.3	1.7	7.4	4.1	0.1	15.5
800 °C	79.0	1.6	8.6	0.7	0.2	10.0

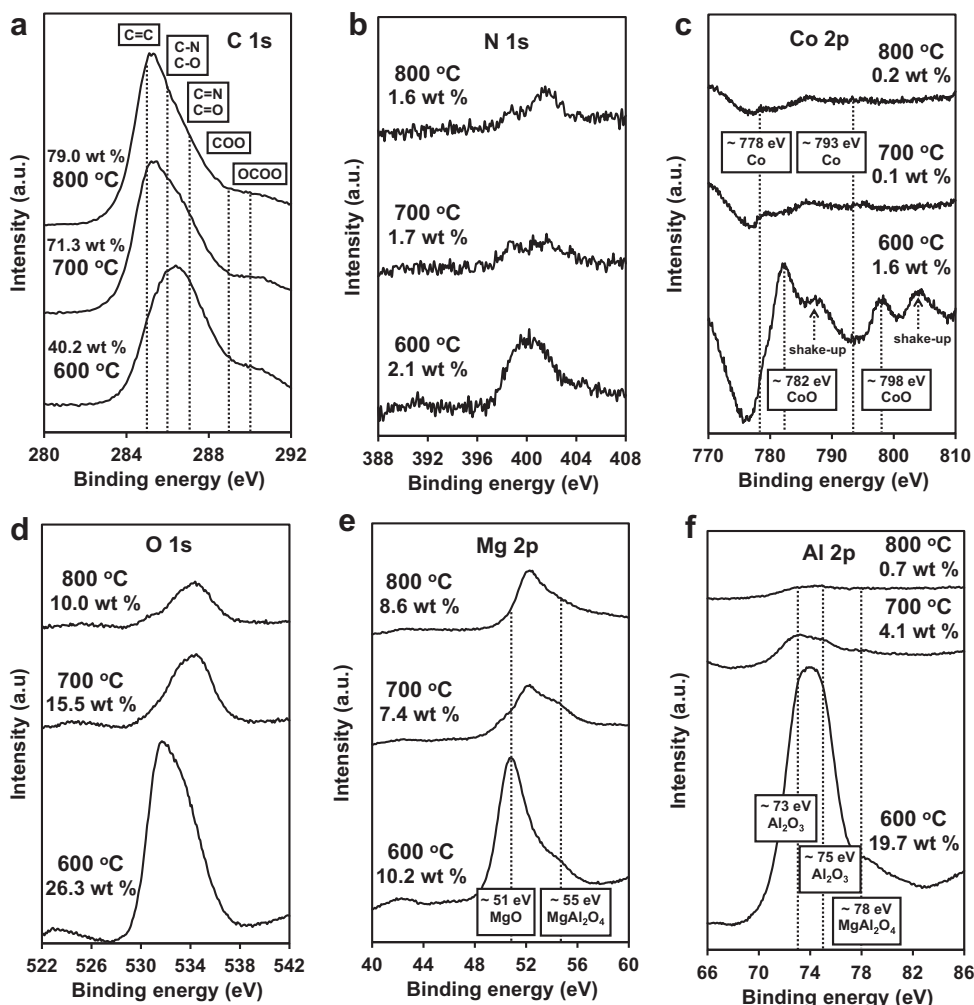
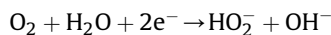


Fig. 7. XPS spectra of the composites prepared at 600, 700 and 800 °C. Surface concentration of particular elements (determined by XPS) is also shown.

increases. The linear relation with  $n = 2$  implies that molecular oxygen undergoes a two-electron reduction according to the following reaction:



The deviation at higher rotation rates suggests the presence of additional process inhibiting the oxygen transport. The most plausible inhibiting process is the transport within the catalyst pores. This is reasonable because the deviation starts at lower rotation rate for the composite prepared at 700 °C, which has higher porosity than that prepared at 800 °C.

The ability of the catalysts studied in the present study to reduce oxygen results from a coexistence of cobalt species and N-doped graphite-like carbon. It has been reported that oxygen reduction reaction through a two-electron pathway is catalyzed equally by Co- and carbon-containing electrocatalysts [12,13,52,53].

The nature of the catalytic sites existing in studied electrode materials remains uncertain because we are not able to assign them precisely based on the experimental data but we propose a few surroundings possibly occurring in our catalytic systems which may be (part of) active sites.

Certain forms of cobalt may act as active sites [11]. Cobalt nanoclusters may be responsible for observed catalytic activity for ORR [12]. However, not the whole range of cobalt dispersed in the catalysts is accessible for electrode process.

Cobalt ions coordinated with nitrogen, which have been claimed to be active in ORR, are also suspected to be formed during CCVD and participate in ORR. We are not capable of confirming the existence of such species. More advanced techniques including ToF-SIMS (time-of-flight secondary ion mass spectroscopy, XAS (X-ray absorption spectroscopy) and Mössbauer spectroscopy should be employed to detect Co–N bonding [11,12]. We cannot exclude the possibility of the existence of cobalt and nitrogen bonded together especially that thermal treatment of acetonitrile generates nitrogen containing surface groups that may serve as coordination centers for cobalt ions.

The carbon-rich component mainly in form of carbon nanotubes, possessing functional (N- and O-containing) groups may play an important role in observed catalytic activity for ORR. Nitrogen atoms incorporated in the carbon framework especially pyridine-like nitrogen may make an important contribution to the catalytic activity of the electroactive composites. Formation of pyridinic nitrogen atoms is often observed on the edge of the graphite plane, and the lone pair of electrons from pyridine-like nitrogen has been attributed to ORR activity [54]. Since nitrogen-containing groups on the outermost wall are more important for ORR, it suggests that quaternary nitrogen formed on the inner wall in N-doped CNTs has less impact on ORR [19].

The presence of nitrogen in carbon matrixes enhances the catalytic activity of carbons in electron transfer reactions because

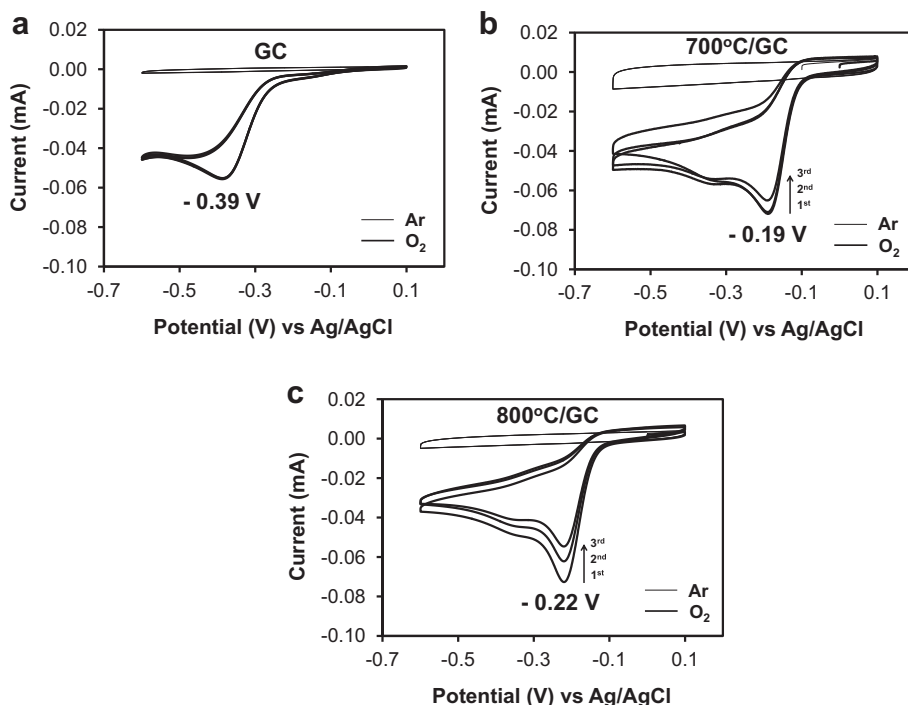


**Fig. 8.** CVs recorded in an oxygen- or argon-saturated 0.1 M KOH solutions with a sweep rate of  $10 \text{ mV s}^{-1}$  at (a) a bare GC and GC coated with the catalysts prepared at (b) 700 and (c) 800 °C.

replacing carbon with nitrogen improves the ability of graphite to donate electrons to oxygen or other reactants [55,56]. The influence of nitrogen on the catalytic properties of N-doped graphite-like carbons may be explained assuming that the insertion of nitrogen atoms into the graphite lattice lowers the band gap width, thus producing higher electron (charge) mobility and a lowering the electron work function at the carbon/liquid (gas) interface compared with pure carbons [57]. Quantum chemical calculations reported by Strelko et al. [57] show that the combination of pyrrolic and pyridinic nitrogen atoms yields carbons with the minimum band gap.

Besides providing adsorption sites for physical or specific adsorption, carbon matrix, which has pores with a certain size distribution and functional groups, is able to catalyze surface reactions [58]. The catalytic activity of nitrogen-containing carbons is often associated with their basic properties, since nitrogen-doping produces enhanced basicity. Electrons are transferred from the catalyst to adsorbed oxygen molecules producing highly reactive species, e.g. radicals [58,59].

Besides nitrogen substituted in the carbon framework, oxygen being also incorporated in carbon matrixes has a certain impact on

the catalytic properties of the composites. According to quantum chemical calculations, replacing carbon with oxygen, especially by introduction of oxygen atoms in the form of  $\text{C}=\text{O}$  into the carbon framework lowers the ability of graphite-like carbon to donate electrons to reactants (oxygen) [60]. On the other hand, oxygen atoms located in the carbon matrix are involved in ORR as mediators; therefore they play an essential role in studied electrode process. The two-electron reduction of  $\text{O}_2$  to  $\text{HO}_2^-$  is mediated by oxygen-containing groups (so called quinone-like groups) on carbon surface, e.g. glassy carbon, carbon nanotubes, graphene [2,61,62]. The contribution of oxide part in the composites, estimated by TG analysis, is substantial. The proportion of oxide part to carbon part in the composites is relatively high and equal to 1.6:1 and 0.8:1 for the samples prepared at 700 and 800 °C, respectively. It seems that surface oxygen concentration determined by XPS analysis relates not only to oxygen-containing groups associated with the carbon matrix but also to metal oxides, e.g.  $\text{MgO}$ ,  $\text{Al}_2\text{O}_3$  and  $\text{MgAl}_2\text{O}_4$ . Therefore, information on oxygen content in the electrocatalysts is not taken into consideration.

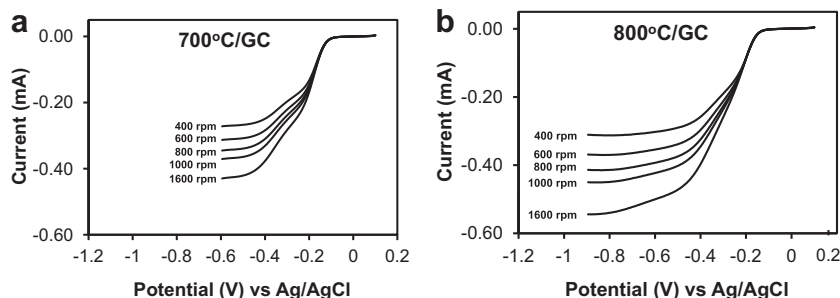


**Fig. 9.** The current–potential relations recorded in an oxygen-saturated 0.1 M KOH solution by sweeping the potential at  $5 \text{ mV s}^{-1}$  for a GC coated with the catalysts prepared at (a) 700 and (b) 800 °C at various rotation rates.

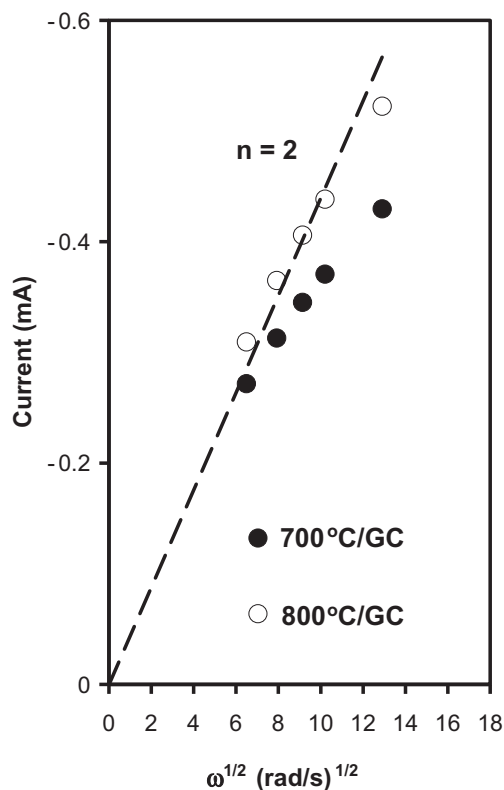


Fig. 10. The Levich plots for oxygen reduction reaction over a GC coated with the catalysts prepared at (full circles) 700 and (empty circles) 800 °C.

In order to confirm the two-electron reduction process over the catalysts prepared at 700 and 800 °C we apply the analysis based on Koutecky–Levich (K.–L.) equation:

$$i^{-1} = i_k^{-1} + \left(0.62nFAD^{2/3}C_v^{-1/6}\omega^{1/2}\right)^{-1} = i_k^{-1} + B^{-1}\omega^{-1/2}$$

where  $i$  is the measured current and  $i_k$  is the current controlled by electron transfer kinetics.

Fig. 11 shows the K.–L. plots at various potentials for a GC coated with electrocatalysts prepared at 700 and 800 °C. The graphs of the inverse of current against the inverse of the square root of the rotation rate of the electrode, at different potentials have a nearly constant slope, meaning that the reduction of oxygen is irreversible and of first order with respect to oxygen concentration. The kinetic current ( $i_k$ ) of ORR can be obtained from the intercept of the K.–L. plots for various potentials and then the kinetic rate constant ( $k$ ) of ORR (shown in Table 4) is obtained by the following equation [63]:

$$i_k = nFAkC$$

Fig. 12 shows Tafel plots of mass-transport-corrected currents at GC electrode coated with the composites. The kinetic currents free of mass transfer effects are obtained from the intercepts of the K.–L. plots. Two Tafel slopes are observed, e.g. –64 or –65 mV per decade in lower current region for the catalysts prepared at 700 and 800 °C, respectively, and –125 or –128 mV per decade in higher current region for the catalysts prepared at 700 and 800 °C, respectively. According to previous studies, the Tafel slope for platinum based electrodes in alkaline solution is close to –60 mV per decade in low current region and –120 mV per decade in high current region [64]. The presence of two slopes corresponds to low and high oxygen

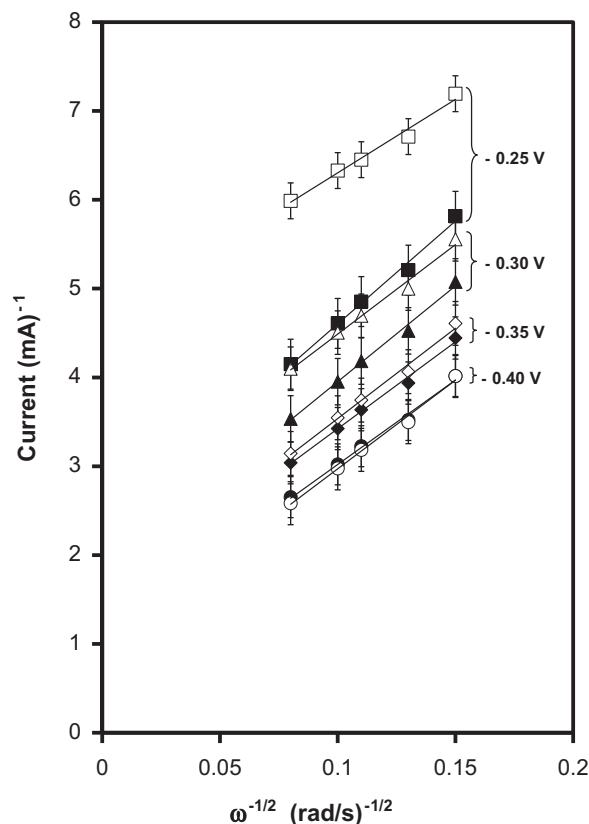


Fig. 11. The Koutecky–Levich plots for the polarization curves (Fig. 9) of the catalysts prepared at (full symbols) 700 and (empty symbols) 800 °C deposited on a GC electrode.

coverage and therefore different oxygen adsorption mechanisms. Molecular oxygen adsorbs onto the catalysts following the Temkin adsorption isotherm in low current region (high coverage), whereas in high current region, molecular oxygen adsorbs onto the catalysts following the Langmuir adsorption isotherm (low coverage). The presence of two Tafel slopes may suggest similar oxygen adsorption mechanisms existing in studied electrocatalysts as in the case of platinum and/or N-doped carbon nanotubes containing catalysts [16,65]. Since the Tafel slopes for two electrodes are comparable, oxygen reduction reaction mechanism may be considered to be the same and the main difference between the electrocomposites should be in the concentration of the active sites.

Since the electrode materials have a complex composition with different contribution of the components, the interface area between the electrode and the electrolyte is inhomogeneous, which may affect oxygen adsorption process and oxygen reduction reaction. Only certain atoms and/or group of atoms existing on the surface of the composites are active in ORR being a multi-step reaction. Despite the electrode materials have comparable porosity (pore size and pore volume) determined by nitrogen sorption, they indicate different electrode/electrolyte contact area. For example, the composite prepared at lower temperature consists of smaller particles and contains carbon matrix with higher density of edge plane sites, which provides larger electrode/electrolyte interface area reflecting in higher capacitance [35,49].

The composite prepared at higher temperature may indicate lower concentration of lattice defects associated with active sites, which are beneficial to ORR [10]. Maldonado and Stevenson [23] demonstrated that nitrogen-containing carbon possesses significantly more defects than pure carbon prepared under similar

**Table 4**Comparison of the Koutecky–Levich data (mean  $\pm$  standard deviation for four determinations) of the catalysts prepared at 700 and 800 °C deposited on GC.

700 °C/GC <sup>-1</sup>				800 °C/GC <sup>-1</sup>			
Potential (V)	Electron number	Kinetic current (mA)	Rate constant (cm s <sup>-1</sup> ) $\times 10^3$	Potential (V)	Electron number	Kinetic current (mA)	Rate constant (cm s <sup>-1</sup> ) $\times 10^3$
-0.25	2.0 $\pm$ 0.1	0.44 $\pm$ 0.04	9.5 $\pm$ 1.0	-0.25	2.9 $\pm$ 0.1	0.21 $\pm$ 0.03	3.2 $\pm$ 0.3
-0.30	2.1 $\pm$ 0.1	0.56 $\pm$ 0.07	11.7 $\pm$ 1.5	-0.30	2.3 $\pm$ 0.1	0.40 $\pm$ 0.04	7.6 $\pm$ 0.5
-0.35	2.3 $\pm$ 0.1	0.70 $\pm$ 0.09	13.0 $\pm$ 1.3	-0.35	2.3 $\pm$ 0.1	0.66 $\pm$ 0.03	12.7 $\pm$ 0.6
-0.40	2.4 $\pm$ 0.1	0.90 $\pm$ 0.15	16.4 $\pm$ 2.0	-0.40	2.3 $\pm$ 0.1	1.02 $\pm$ 0.03	19.2 $\pm$ 1.4

conditions and that only nitrogen-doped carbon has good activity for ORR in alkaline solutions. Furthermore, N- and O-containing groups may also affect the physical adsorption of oxygen [58]. Nitrogen creates defects in carbon layers, which leads to increase edge plane exposure [66]. However, edge plane exposure alone does not lead to improved activity for ORR for carbon without nitrogen doping. Carbon structures (not containing nitrogen) with edge plane exposure have not high activity for ORR. Defective and rough carbon matrix may facilitate oxygen adsorption.

Synthesis temperature influences metallic cobalt dispersion in the composites. XRD analysis reveals an increase in cobalt particle size with increasing synthesis temperature. According to XPS analysis, the electrocatalysts have different surface cobalt concentration, which is twofold lower for the sample prepared at 700 °C than for that prepared at 800 °C. The catalytic activity of the electroactive composites does not correlate with metallic cobalt concentration, which implies that cobalt itself is not a primary source of activity.

The treatment of the catalysts with acid leads to get rid of metal oxides, e.g. MgO and partial dissolution of cobalt species especially those not being occluded by carbon deposit. According to preliminary CV data, acid-treated catalysts are also active in ORR. The reduction peaks are observed at -0.16 and -0.18 V in the CVs recorded for the acid-treated catalysts prepared at 700 and 800 °C, respectively. It shows that despite they contain less net amount of cobalt and perhaps only cobalt being encapsulated in carbon nanotubes, they become even more active in ORR than the as-prepared catalysts. Moreover, acid treatment results in increase in the catalyst porosity. Pore volume determined by nitrogen sorption increases from 0.07 to 0.08 cm<sup>3</sup> g<sup>-1</sup> for the as-prepared catalysts obtained at 700 and 800 °C, respectively, to 0.63 and 0.32 cm<sup>3</sup> g<sup>-1</sup> for the acid-treated catalysts obtained at 700 and 800 °C, respectively. The capacitances for the acid-treated composites prepared at 700 and 800 °C are ca. 28 and 15 F g<sup>-1</sup>, respectively. It seems that the acid-treated catalysts have developed electrode/electrolyte

interface area with improved access to the catalytic sites. According to TG analysis carbon-rich component (with incorporated N- and O-containing groups) content in the catalysts before treating with acid is 38 and 57 wt %, whereas in the catalysts after treating with acid is 86 and 85 wt %, for samples prepared at 700 and 800 °C, respectively. Acid treatment by lowering metal/metal oxide content in the composites leads to increase in carbon-rich component (with embedded cobalt nanoclusters) contribution to the acid-treated catalysts. The acid-treated catalysts possess enhanced active surface area as they have developed electrode/electrolyte interface area and higher concentration of active sites than the as-prepared catalysts.

#### 4. Conclusions

The electrocatalysts for oxygen reduction reaction containing cobalt and N-doped graphite-like carbon were prepared via the simultaneous decomposition of Mg–Co–Al layered double hydroxides and acetonitrile at various synthesis temperatures. Application of different synthesis temperature influences the concentration, the level of graphitization, the extent of N-doping and the morphology of graphite-like carbon in the composites, which mainly determine electrode/electrolyte interface active area important for ORR. Electrochemical measurements in 0.1 M KOH solution at a glassy carbon electrode modified with the composites prepared at 700 and 800 °C proves that ORR at these electrodes proceeds by 2-electron pathway.

#### Acknowledgments

This work was financially supported by World Premier International Research Center (WPI) Initiative on Materials Nano-architectonics from the Ministry of Education, Culture, Sports, Science and Technology (MEXT), Japan. Prof. Katsuaki Shimazu and Dr. Toshikazu Kawaguchi (Hokkaido University) are gratefully acknowledged for XPS measurements.

#### References

- [1] Z. Mo, S. Liao, Y. Zheng, Z. Fu, Carbon 50 (2012) 2620–2627.
- [2] J. Wu, D. Zhang, Y. Wang, Y. Wan, B. Hou, J. Power Sources 198 (2012) 122–126.
- [3] Y. Wang, D. Zhang, H. Liu, J. Power Sources 195 (2010) 3135–3139.
- [4] L. Zhang, F. Li, Appl. Clay Sci. 50 (2010) 64–72.
- [5] T. Stimpfling, F. Leroux, Chem. Mater. 22 (2010) 974–987.
- [6] X. Deng, X. Wang, Z.-F. Ma, J. Power Sources 183 (2008) 604–608.
- [7] Z. Fan, J. Chen, K. Cui, F. Sun, Y. Xu, Y. Kuang, Electrochim. Acta 52 (2007) 2959–2965.
- [8] G. Wei, J.S. Wainright, R.F. Savinell, J. New Mater. Electrochem. Syst. 3 (2000) 121–129.
- [9] C.W.B. Bezerra, L. Zhang, K. Lee, H. Liu, A.L.B. Marques, E.P. Marques, H. Wang, J. Zhang, Electrochim. Acta 53 (2008) 4937–4951.
- [10] H. Qin, S. Lao, Z. Liu, J. Zhu, Z. Li, Int. J. Hydrogen Energy 35 (2010) 1872–1878.
- [11] G. Faubert, G. Lalande, R. Côté, D. Guay, J.P. Dodelet, L.T. Weng, P. Bertrand, G. Dénès, Electrochim. Acta 41 (1996) 1689–1701.
- [12] A.L. Bouwkamp-Wijnoltz, W. Visscher, J.A.R. van Veen, S.C. Tang, Electrochim. Acta 45 (1999) 379–386.
- [13] M. Mamlouk, S.M.S. Kumar, P. Gouerec, K. Scott, J. Power Sources 196 (2011) 7594–7600.

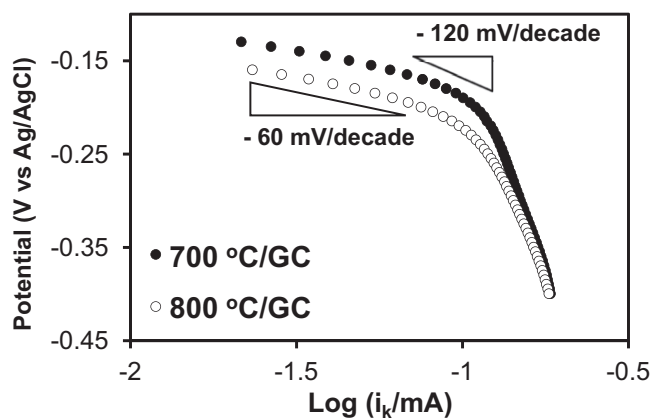


**Fig. 12.** The Tafel plots for oxygen reduction reaction at a GC coated with the composites prepared at (full circles) 700 and (empty circles) 800 °C in 0.1 M KOH solution.

- [14] H.Y. Qin, K.N. Zhu, L.Q. Ye, Z.P. Li, J. Power Sources 208 (2012) 203–209.
- [15] W.Y. Wong, W.R.W. Daud, A.B. Mohamad, A.A.H. Kadhum, E.H. Majlan, K.S. Loh, Diamond Relat. Mater. 22 (2012) 12–22.
- [16] Z. Chen, D. Higgins, Z. Chen, Carbon 48 (2010) 3057–3065.
- [17] Y. Tang, B.L. Allen, D.R. Kauffman, A. Star, J. Am. Chem. Soc. 131 (2009) 13200–13201.
- [18] K. Gong, F. Du, Z. Xia, M. Durstock, L. Dai, Science 323 (2009) 760–764.
- [19] Z. Chen, D. Higgins, H. Tao, R.S. Hsu, Z. Chen, J. Phys. Chem. C 113 (2009) 21008–21013.
- [20] S. Kundu, T.C. Nagaiah, W. Xia, Y. Wang, S. Dommele, J.H. Bitter, M. Santa, G. Grundmeier, M. Bron, W. Schuhmann, M. Muhler, J. Phys. Chem. C 113 (2009) 14302–14310.
- [21] Y. Shao, J. Sui, G. Yin, Y. Gao, Appl. Catal. B Environ 79 (2008) 89–99.
- [22] P.H. Matter, E. Wang, M. Arias, E.J. Biddinger, U.S. Ozkan, J. Phys. Chem. B 110 (2006) 18374–18384.
- [23] S. Maldonado, K.J. Stevenson, J. Phys. Chem. B 109 (2005) 4707–4716.
- [24] F. Li, Q. Tan, D.G. Evans, X. Duan, Catal. Lett. 99 (2005) 151–156.
- [25] H.I. Hima, X. Xiang, L. Zhang, F. Li, J. Mater. Chem. 18 (2008) 1245–1252.
- [26] R. Xue, Z. Sun, L. Su, X. Zhang, Catal. Lett. 135 (2010) 312–320.
- [27] M.-Q. Zhao, Q. Zhang, J.-Q. Huang, J.-Q. Nie, F. Wei, Carbon 48 (2010) 3260–3270.
- [28] File No. 00-048-1719 of JCPDS-ICDD diffraction database PDF-2.
- [29] File No. 00-071-3631 of JCPDS-ICDD diffraction database PDF-2.
- [30] File No. 00-071-4238 of JCPDS-ICDD diffraction database PDF-2.
- [31] File No. 00-058-1638 of JCPDS-ICDD diffraction database PDF-2.
- [32] File No. 00-073-1959 of JCPDS-ICDD diffraction database PDF-2.
- [33] H. Darmstadt, C. Roy, S. Kaliaguine, S.J. Choi, R. Ryoo, Carbon 40 (2002) 2673–2683.
- [34] C.-M. Chen, Y.-M. Dai, J.G. Huang, J.-M. Jehng, Carbon 44 (2006) 1808–1820.
- [35] W. Jiang, G. Nadeau, K. Zaghib, K. Kinoshita, Thermochim. Acta 351 (2000) 85–93.
- [36] M. Kruk, M. Jaroniec, Chem. Mater. 13 (2001) 3169–3183.
- [37] K.B.K. Teo, C. Singh, M. Chhowalla, W.I. Milne, Catalytic synthesis of carbon nanotubes and nanofibers, in: H.S. Nalwa (Ed.), Encyclopedia of Nanoscience and Nanotechnology, vol. 10, American Scientific Publishers, California, 2003, pp. 1–22.
- [38] R.K. Rana, X.N. Xu, Y. Yeshurun, A. Gedanken, J. Phys. Chem. B 106 (2002) 4079–4084.
- [39] M. Pakula, S. Biniak, A. Świątkowski, S. Neffe, Carbon 40 (2002) 1873–1881.
- [40] S. Ardizzone, C.L. Bianchi, M. Fadoni, B. Vercelli, Appl. Surf. Sci. 119 (1997) 253–259.
- [41] K.Y. Park, J.G. Choi, K. Sung, Y. Kim, J. Nanopart. Res. 8 (2006) 1075–1081.
- [42] I.V. Plyuto, A.P. Shpak, I.V. Babich, Y.V. Plyuto, L.F. Sharanda, J. Stoch, J.A. Moulijn, Surf. Interface Anal. 27 (1999) 911–914.
- [43] B.J. Tan, K.J. Klabunde, P.M.A. Sherwood, J. Am. Chem. Soc. 113 (1991) 855–861.
- [44] A. Świątkowski, H. Grajek, M. Pakula, S. Biniak, Z. Witkiewicz, Colloid Surf. A 208 (2002) 313–320.
- [45] A. Rizzetti, J. Xhie, K. Sattler, D. Yamamoto, W. Pong, J. Electron. Spectrosc. 58 (1992) 359–364.
- [46] D. Barreca, C. Massignan, S. Daolio, M. Fabrizio, C. Piccirillo, L. Armelao, E. Tondello, Chem. Mater. 13 (2001) 588–593.
- [47] P.A. Chernavskii, A.Y. Khodakov, G.V. Pankina, J.-S. Girardon, E. Quinet, Appl. Catal. A Gen. 306 (2006) 108–119.
- [48] A.F. Lucrédio, G.T. Filho, E.M. Assaf, Appl. Surf. Sci. 255 (2009) 5851–5856.
- [49] T. Kim, S. Lim, K. Kwon, S.-H. Hong, W. Qiao, C.K. Rhee, S.-H. Yoon, I. Mochida, Langmuir 22 (2006) 9086–9088.
- [50] V.S. Bagotsky, Fundamentals of Electrochemistry, second ed., John Wiley & Sons, Inc., Hoboken, New Jersey, 2006.
- [51] N. Alexeyeva, E. Shluga, V. Kisand, I. Kink, K. Tammeveski, J. Electroanal. Chem. 648 (2010) 169–175.
- [52] N. Alexeyeva, K. Tammeveski, Electrochem. Solid-State Lett. 10 (2007) F18–F21.
- [53] V. Bambagioni, C. Bianchini, J. Filippi, A. Lavacchi, W. Oberhauser, A. Marchionni, S. Moneti, F. Vizza, R. Psaro, V. Dal Santo, A. Gallo, S. Recchia, L. Sordelli, J. Power Sources 196 (2011) 2519–2529.
- [54] R.A. Sidik, A.B. Anderson, N.P. Subramanian, S.P. Kumaraguru, B.N. Popov, J. Phys. Chem. B 110 (2006) 1787–1793.
- [55] S. Maldonado, S. Morin, K.J. Stevenson, Carbon 44 (2006) 1429–1437.
- [56] B. Stöhr, H.P. Boehm, R. Schlögl, Carbon 29 (6) (1991) 707–720.
- [57] V.V. Strelko, V.S. Kuts, P.A. Thrower, Carbon 38 (2000) 1499–1524.
- [58] P. Serp, J.L. Figueiredo (Eds.), Carbon Materials for Catalysis, first ed., John Wiley & Sons, Inc., Hoboken, New Jersey, 2009.
- [59] S. Biniak, M. Walczyk, G.S. Szymański, Fuel Process. Technol. 79 (2002) 251–257.
- [60] V.V. Strelko, N.T. Kartel, I.N. Dukhno, V.S. Kuts, R.B. Clarkson, B.M. Odintsov, Surf. Sci. 548 (2004) 281–290.
- [61] M. Zhang, Y. Yan, K. Gong, L. Mao, Z. Guo, Y. Chen, Langmuir 20 (2004) 8781–8785.
- [62] T. Ohsaka, L. Mao, K. Arihara, T. Sotomura, Electrochem. Commun. 6 (2004) 273–277.
- [63] M. Harada, H. Noguchi, N. Zanetakis, S. Takakusagi, W. Song, K. Uosaki, Sci. Technol. Advan. Mater. 12 (2011) 044606–044616.
- [64] N. Alexeyeva, K. Tammeveski, A. Lopez-Cudero, J. Solla-Gullón, J.M. Feliu, Electrochim. Acta 55 (2010) 794–803.
- [65] A. Kongkanand, S. Kuwabata, G. Girishkumar, P. Kamt, Langmuir 22 (2006) 2392–2396.
- [66] P.H. Matter, L. Zhang, U.S. Ozkan, J. Catal. 239 (2006) 83–96.